3D MRI atlases of congenital aortic arch anomalies and normal fetal heart: application to automated multi-label segmentation

Alena Uus[1], Milou P.M. van Poppel[1,2], Johannes K. Steinweg[1,3], Irina Grigorescu[1], Alexia Egloff Collado[3], Paula Ramirez Gilliland[1], Thomas A. Roberts[1,4], Joseph V. Hajnal[1,3], Mary A. Rutherford[3], David F.A. Lloyd[1,2], Kuberan Pushparajah[1,2], Maria Deprez[1]

1: School of Imaging Sciences & Biomedical Engineering, King's College London, St. Thomas' Hospital, London, SE1 7EH, UK

2: Department of Congenital Heart Disease, Evelina London Children's Hospital, London, SE1 7EH, UK

3: Centre for the Developing Brain, King's College London, London, SE1 7EH, UK

4: Clinical Scientific Computing, Guy's and St Thomas' NHS Foundation Trust, London, UK

Abstract

The black blood contrast T2w ssFSE fetal MRI along with application of 3D slice-to-volume registration methods allows reconstruction of high-resolution 3D images of the heart that provide superior visualisation of fetal cardiovascular anomalies. However, there is a lack of formalisation of the MRI appearance of fetal cardiovascular anatomy and standardisation of vessel segmentation protocols.

In this work, we present the first 3D fetal MRI atlases defining normal and abnormal fetal cardiovascular anatomy. We also perform evaluation of the feasibility of atlas-guided registration and deep learning methods for automated 3D multi-label vessel segmentation.

Introduction

The black blood contrast in T2w ssFSE fetal MRI provides superior visualisation of fetal cardiovascular anomalies [1]. Recently, application of slice-to-volume registration (SVR) motion correction tools [2] for reconstruction of high-resolution 3D T2w images of the fetal heart was shown to provide adjunct diagnostic information [3] and allow visualisation of the fetal extracardiac vasculature using 3D models.

At our institution, the main referral indications for 3D T2w fetal cardiac MRI (CMR) [3] include suspected coarctation of the aorta (CoA), right aortic arch (RAA) with aberrant left subclavian artery (ALSA) and suspected double aortic arch (DAA). However, despite the reported improved diagnostic performance of 3D fetal CMR [3,4], there is a lack of formalization of the MRI appearance of fetal cardiovascular anatomy. Furthermore, currently, 3D semi-automatic segmentation of fetal vasculature from T2w SVR images [3] requires time-consuming manual refinement, especially for multiple labels and is vulnerable to inter-observer bias.

In this work, we present the first 3D fetal MRI atlases defining normal and abnormal (suspected CoA, RAA+ALSA, DAA) fetal cardiovascular anatomy generated from 87 fetal CMR datasets along with the formalised multi-label parcellations of the major cardiovascular structures. This could potentially contribute to standardisation of the 3D SVR-based diagnostic protocol and quantitative analysis. We also perform evaluation of the feasibility of atlas-guided registration and deep learning methods for automated 3D multi-label vessel segmentation.

Method

Datasets and preprocessing: The fetal MRI data include 87 datasets acquired under the iFIND [5] project at St. Thomas's Hospital, London [REC: 14/LO/1806] and as a part of the fetal CMR service at Evelina London Children's Hospital, with data use for this project subject to informed consent of the participants [REC: 07/H0707/105]. The cohorts (Fig.1A) include 29 fetuses without reported cardiac anomalies ("normal"), 58 cases with postnatally confirmed abnormality (20 CoA, 21 RAA and 17 DAA). The inclusion criteria were high SNR, 29-34 weeks gestational age (GA) and absence of other cardiovascular anomalies. The acquisitions were performed on a 1.5T Philips Ingenia MRI system using torso receiver array and T2w ssFSE: TR=15000ms, TE=80ms, voxel size 1.25x1.25x2.5mm, slice thickness 2.5mm and spacing 1.25mm with 9-11 stacks. The 3D reconstructions of the fetal thorax (0.75mm isotropic resolution, standard radiological space) were generated using our new automated deformable SVR (DSVR) pipeline [6,7,8].

Generation of 3D heart atlases with vessel segmentations: The 3D atlases for each of the groups (normal, CoA, RAA+ALSA, DAA) were generated using MIRTK atlas tool [9,10] with 0.6mm output isotropic resolution (Fig.1B). For each of the atlases, a clinician (MVP) trained in fetal CMR manually segmented parcellations of 19 main cardiovascular structures in ITK-SNAP [11]. The chosen structures follow the standard (fetal) CMR reporting. The atlases are publicly available at [12].

Automated segmentation of the fetal heart vessels: A pipeline for automated multi-label 3D segmentation of the cardiovascular structures in 3D DSVR MRI images was implemented in Pytorch MONAI [13] based on of the UNETR transformer-based convolutional neural network (CNN) [14]. We used 39 cases for training and 4 for validation from both normal and CoA cohorts. The preprocessing included cropping to the extracardiac vessel ROI (e.g., Fig.4A), affine registration to the atlas space and resampled with padding to 128x128x128 grid. The labels (13 different vessels) were generated using MIRTK registration-guided cohort-specific atlas label propagation (LP). All labels were visually assessed and confirmed to be qualitatively acceptable. The training was performed for 50000 iterations with MONAI-based augmentation (bias field, contrast adjustment and rotations). The performance was tested on 6 CoA datasets vs. atlas propagated labels in terms of the vessel detection status (visual assessment: correct=100%, partial=50%, failed=0%) and Dice.

Results and Discussion

3D atlases: Fig.2 shows the generated 3D T2w atlases and the corresponding multi-label parcellations. The difference in the relative position of the trachea and the aortic arch(es) and aortic branching in the RAA and DAA atlases vs. the normal anatomy can be clearly seen in the corresponding 3D models (Fig.3A). [15]. The CoA atlas has a pronounced narrowing of the aortic arch (Fig.3B) [2,3]. Importantly, the CoA atlas represents an averaged state of all CoA types as the input cases had varying position and degree of arch narrowing. The anatomical accuracy of the atlases and the segmented structures were confirmed by a clinician with 4 years of fetal CMR experience.

Automated vessel segmentation: The comparison between the automated outputs of the CNN vs. LP methods is summarised in Fig.4C. Similarly, to the classical LP, UNETR CNN correctly detected all vessel in all test CoA subjects (100%) which is confirmed by high specificity. Notably, the registration propagated labels are prone to inconsistencies and cannot be considered as an absolute ground truth. This, along the small vessel size and the partial volume effect, contributed to the lower Dice and sensitivity values for certain vessels (e.g., BCA). The examples in Fig.5 demonstrate that while the global vessel anatomy looks similar, UNETR CNN segmentations have smoother boundaries and correct minor LP errors. This also confirms the feasibility of using atlas LP outputs for CNN training.

Conclusions

This work introduces the first set of 3D black blood T2w MRI atlases of the normal and abnormal fetal vascular anatomy along with detailed segmentation of the major cardiovascular structures. This is a first step towards

standardisation of the processing protocol for fetal cardiovascular anomalies using 3D motion-corrected T2w MRI. We also demonstrated the feasibility of using deep learning for multi-label vessel segmentation. Our future work will focus on optimisation of the CNN-based segmentation pipeline for a wider range of fetal cardiovascular anomalies.

References

[1] Roy, C. W., van Amerom, J. F. P., Marini, D., Seed, M., & Macgowan, C. K. (2019). Fetal Cardiac MRI: A Review of Technical Advancements. *Topics in Magnetic Resonance Imaging: TMRI*, *28*(5), 235–244.

[1] Kuklisova-Murgasova, M., Quaghebeur, G., Rutherford, M. A., Hajnal, J. v., & Schnabel, J. A. (2012). Reconstruction of fetal brain MRI with intensity matching and complete outlier removal. *Med Image Analysis*, *16*(8), 1550–1564.

[2] Lloyd, D. F. A., Pushparajah, K., Simpson, J. M., van Amerom, J. F., van Poppel, M. P. M., Schulz, A., Kainz, B., Deprez, M., Lohezic, M., Allsop, J., Mathur, S., Bellsham-Revell, H., Vigneswaran, T., Charakida, M., Miller, O., Zidere, V., Sharland, G., Rutherford, M., Hajnal, J., & Razavi, R. (2019). Three-dimensional visualisation of the fetal heart using prenatal MRI with motion-corrected slice-volume registration: a prospective, single-centre cohort study. *The Lancet*, *393*(10181), 1619–1627.

[4] Lloyd, D. F. A., van Poppel, M. P. M., Pushparajah, K., Vigneswaran, T. v., Zidere, V., Steinweg, J., van Amerom, J. F. P., Roberts, T. A., Schulz, A., Charakida, M., Miller, O., Sharland, G., Rutherford, M., Hajnal, J. v., Simpson, J. M., & Razavi, R. (2021). Analysis of 3-Dimensional Arch Anatomy, Vascular Flow, and Postnatal Outcome in Cases of Suspected Coarctation of the Aorta Using Fetal Cardiac Magnetic Resonance Imaging. *Circulation: Cardiovascular Imaging*, *14*(7), 583–593.

[5] "iFIND Project." [Online]. Available: http://www.ifindproject.com/. [Accessed: 01-Dec-2021].

[6] Uus, A., Zhang, T., Jackson, L. H., Roberts, T. A., Rutherford, M. A., Hajnal, J. v, & Deprez, M. (2020). Deformable Slice-to-Volume Registration for Motion Correction of Fetal Body and Placenta MRI. *IEEE Transactions on Medical Imaging*, *39*(9), 2750–2759.

[7] Uus, A., Grigorescu, I., van Poppel, M. P. M., Steinweg, J. K., Roberts, T. A., Rutherford, M. A., Hajnal, J. V., Lloyd, D. F. A., Pushparajah, K., & Deprez, M. (2021). Automated 3D reconstruction of the fetal thorax in the standard atlas space from motion-corrupted MRI stacks for 21-36 weeks GA range. *BioRxiv*, 2021.09.22.461335.

[8] "SVRTK: MIRTK based SVR package for fetal MRI." [Online]. Available: https://github.com/SVRTK/. [Accessed: 01-Dec-2021].

[9] "MIRTK package." [Online]. Available: https://github.com/BioMedIA/MIRTK/. [Accessed: 01-Dec-2021].

[10] Schuh, A., Murgasova, M., Makropoulos, A., Ledig, C., Counsell, S. J., Hajnal, J. v, Aljabar, P., & Rueckert, D. (2014). Construction of a 4D Brain Atlas and Growth Model using Diffeomorphic Registration. *STIA MICCAI 2014*.

[11] "ITK-SNAP tool." [Online]. Available: http://www.itksnap.org/. [Accessed: 01-Nov-2021].

[12] "SVRTK fetal MRI data repository." [Online]. Available: https://gin.g-node.org/SVRTK/fetal_mri_atlases. [Accessed: 01-Dec-2021].

[13] "MONAI framework." [Online]. Available: https://github.com/Project-MONAI/MONAI/. [Accessed: 01-Dec-2021].

[14] Hatamizadeh, A., Tang, Y., Nath, V., Yang, D., Myronenko, A., Landman, B., Roth, H., & Xu, D. (2021). UNETR: Transformers for 3D Medical Image Segmentation. *arXiv:2103.10504.*

[15] van Poppel, M. P. M., Pushparajah, K., Lloyd, D. F. A., Razavi, R., Speggiorin, S., Nyman, A., Simpson, J. M., Zidere, V., & Vigneswaran, T. v. (2020). Insights from fetal cardiac magnetic resonance imaging in double aortic arch. *Ultrasound in Obstetrics & Gynecology*, *56*(4), 636–639.

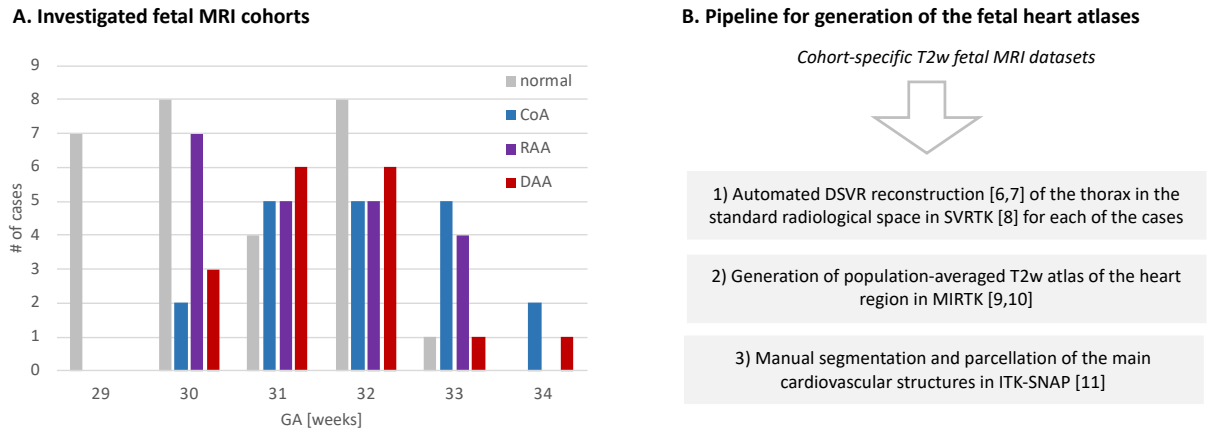

Figure 1. (A) Summary description of the fetal MRI datasets used in this study. (B) The steps for generations of the fetal heart atlases.

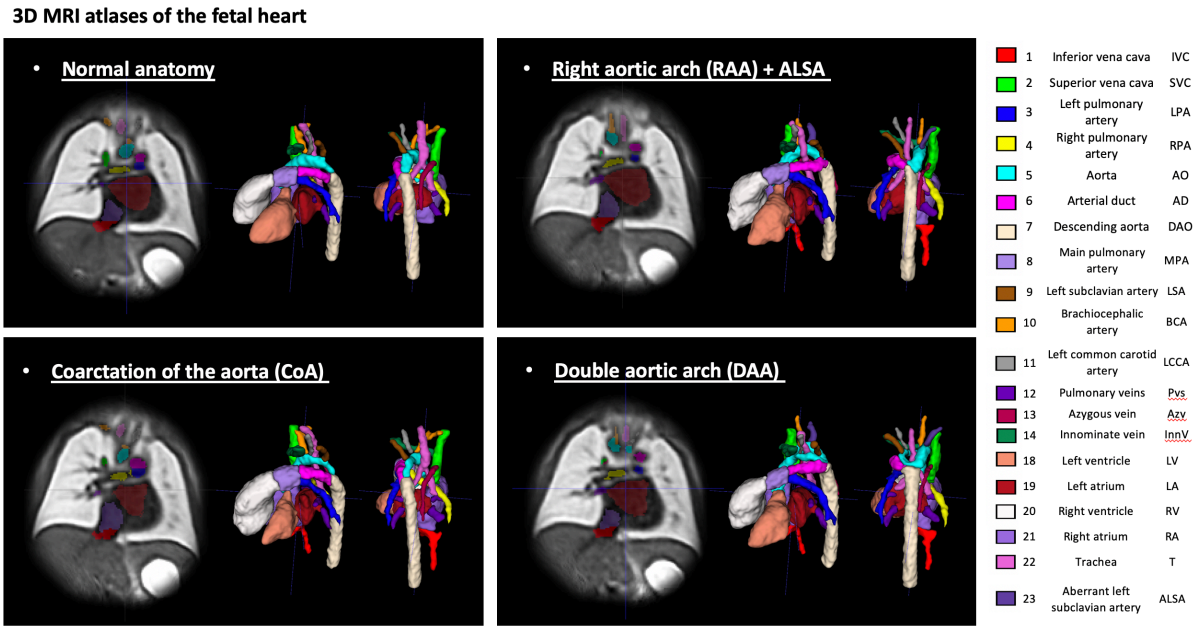

Figure 2. Generated 3D T2w black blood atlases of the normal fetal heart and aortic arch anomalies together with the 3D segmentations of the main 19 cardiovascular structures. The atlases are available at SVRTK fetal MRI data repository [12].

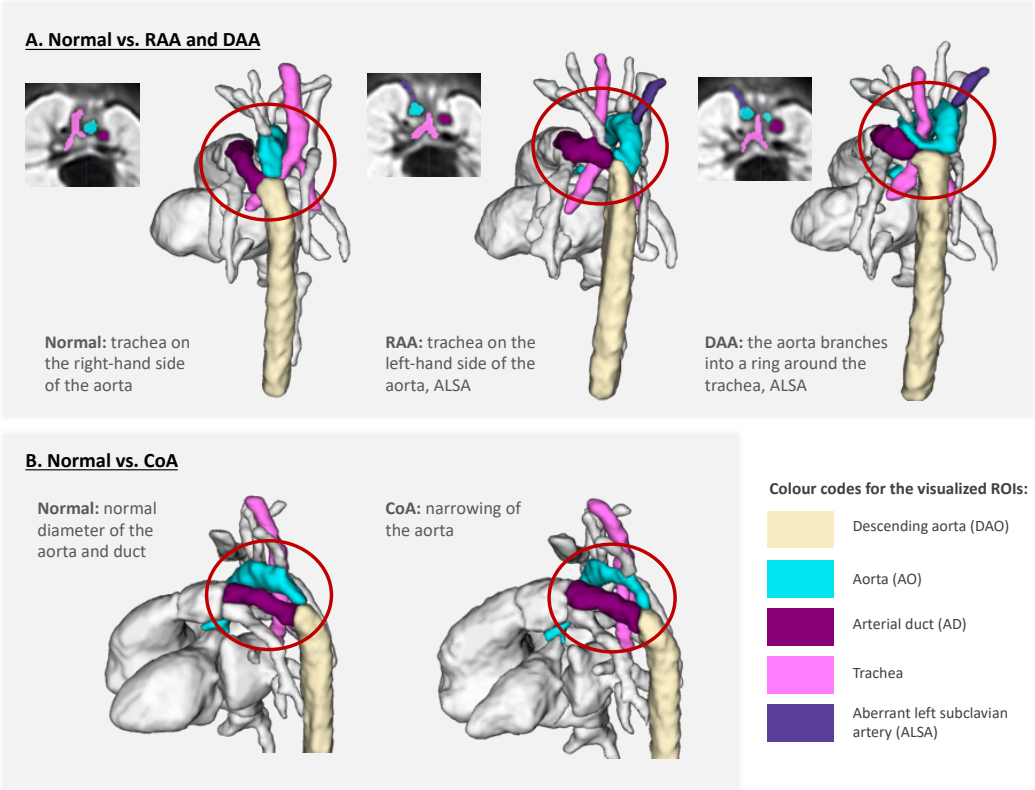

Figure 3. Comparison between normal and abnormal vascular anatomy in the 3D segmentation models of the generated atlases.

Comparison of automated 3D segmentation outputs of label propagation and UNETR CNN: 6 CoA cases in 13 vessel ROIs

A. Investigated 13 vessel ROIs in the CoA atlas space (cropped top part of the heart)

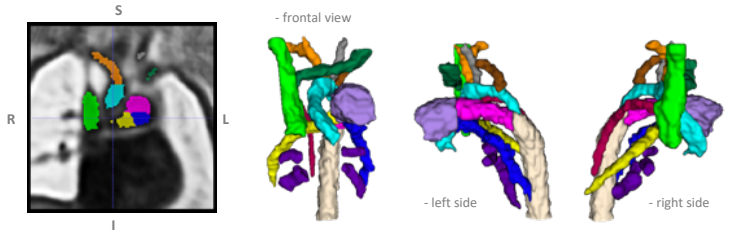

B. Average Dice per vessel ROI

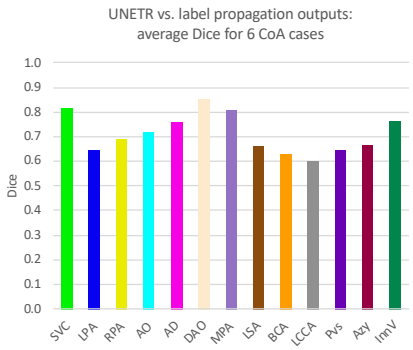

C. Summary table with results: UNETR vs. label propagation outputs

Label in the atlas	Vessel ROI	Abbreviation	Average detection status (UNETR)	Dice	Specificity	Sensitivity
2	Superior vena cava	SVC	100%	0.817 ± 0.054	99.94 ± 0.02 %	81.56 ± 9.90 %
3	Left pulmonary artery	LPA	100%	0.645 ± 0.032	99.95 ± 0.02 %	63.53 ± 3.97 %
4	Right pulmonary artery	RPA	100%	0.692 ± 0.037	99.95 ± 0.01 %	68.96 ± 3.13 %
5	Aorta	AO	100%	0.716 ± 0.039	99.89 ± 0.03 %	76.87 ± 4.98 %
6	Arterial duct	AD	100%	0.761 ± 0.045	99.94 ± 0.03 %	77.02 ± 4.96 %
7	Descending aorta	DAO	100%	0.852 ± 0.022	99.90 ± 0.03 %	89.72 ± 3.94 %
8	Main pulmonary artery	MPA	100%	0.807 ± 0.043	99.91 ± 0.03 %	81.53 ± 5.30 %
9	Left subclavian artery	LSA	100%	0.660 ± 0.050	99.98 ± 0.01 %	68.58 ± 9.88 %
10	Brachiocephalic artery	BCA	100%	0.629 ± 0.026	99.96 ± 0.01 %	73.37 ± 12.22 %
11	Left common carotid artery	LCCA	100%	0.602 ± 0.032	99.99 ± 0.00 %	63.26 ± 11.44 %
12	Pulmonary veins	Pvs	100%	0.644 ± 0.044	99.96 ± 0.01 %	59.31 ± 4.82 %
13	Azygous vein	Azy	100%	0.668 ± 0.061	99.97 ± 0.01 %	63.00 ± 7.52 %
14	Innominate vein	InnV	100%	0.763 ± 0.037	99.96 ± 0.01 %	78.66 ± 5.19 %

Figure 4. Comparison of 3D atlas-based label propagation and UNETR CNN multi-label segmentation outputs for 6 CoA datasets.

A. CoA test case I

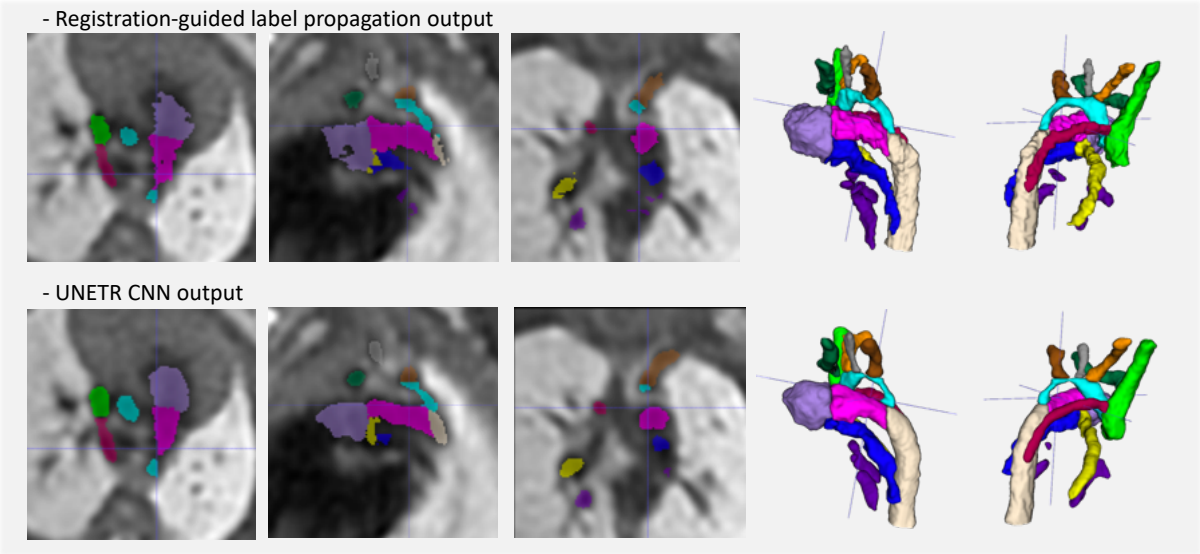

B. CoA test case II

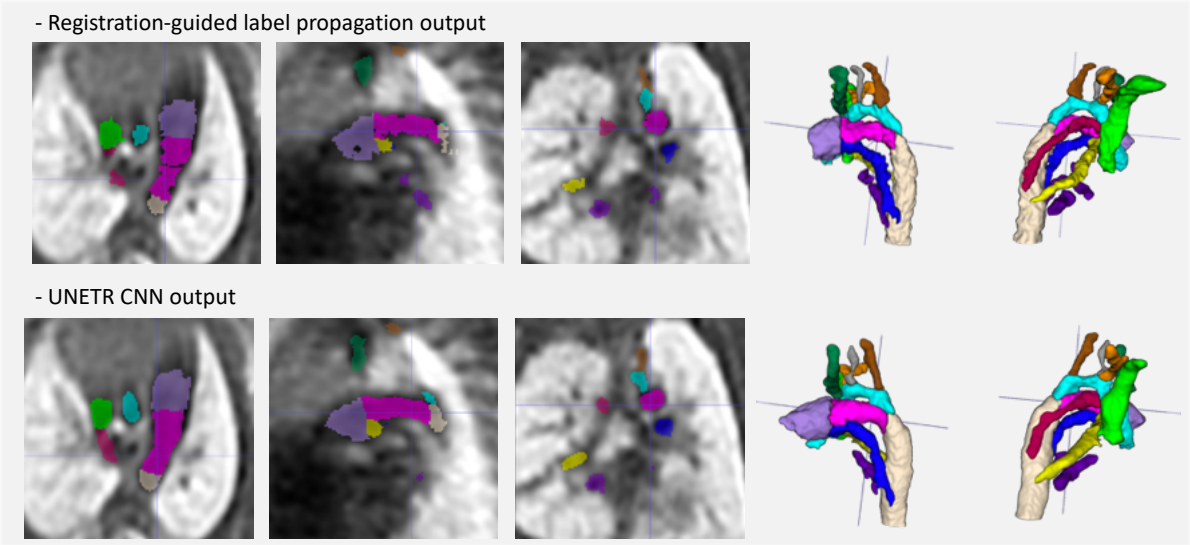

Figure 5. Examples of 3D atlas-based label propagation vs. UNETR CNN automated multi-label segmentation results for two test CoA datasets.